# Integrative genomic analysis identifies unique immune environments associated with immunotherapy response in diffuse large B cell lymphoma

Sravya Tumuluru[1*], James K. Godfrey[2*], Alan Cooper[3], Jovian Yu[3], Xiufen Chen[3], Brendan W. MacNabb[4], Girish Venkataraman[5], Yuanyuan Zha[3], Benedikt Pelzer[6], Joo Song[7], Gerben Duns[8], Brian J. Sworder[9], Christopher Bolen[10], Elicia Penuel[10], Ekaterina Postovalova[11], Nikita Kotlov[11], Aleksander Bagaev[11], Nathan Fowler[11], Sonali M. Smith[3], Ash A. Alizadeh[12], Christian Steidl[8,13], Justin Kline[1,3 #]

**Affiliations**:

[1] Committee on Cancer Biology, University of Chicago, Chicago, IL

[2] Department of Hematology & Hematopoietic Cell Transplantation, City of Hope, Duarte, CA

[3] Department of Medicine, Section of Hematology/Oncology, University of Chicago, Chicago, IL

[4] Division of Biology and Biological Engineering, California Institute of Technology, Pasadena, CA

[5] Department of Pathology, University of Chicago, Chicago, IL

[6] Division of Hematology and Oncology, Weill Cornell Medicine, New York, NY

[7] Department of Pathology, City of Hope, Duarte, CA

[8] Centre for Lymphoid Cancer, BC Cancer, Vancouver, BC, Canada

[9] Division of Hematology/ Oncology, Department of Medicine, University of California – Irvine, Irvine, CA

[10] Genentech Inc., South San Francisco, CA

[11] BostonGene Corporation, Waltham, MA

[12] Division of Oncology, Department of Medicine, Stanford University, Palo Alto, CA

[13] Department of Pathology and Laboratory Medicine, University of British Columbia, Vancouver, BC, Canada

[*] These authors contributed equally

[#] Corresponding author

**Corresponding Author**:
Justin Kline, M.D.
Department of Medicine, Section of Hematology/Oncology, University of Chicago
900 East 57th Street, Chicago, IL, 60637
Phone: (773) 702-5550; Fax: (773) 702-3163; Email: jkline@uchicagomedicine.org

**Word Count:** 4900

**Number of Figures/Tables:** 5

## Abstract

Most diffuse large B-cell lymphoma (DLBCL) patients treated with bispecific antibodies (BsAb) or chimeric antigen receptor (CAR) T cells fail to achieve durable treatment responses, underscoring the need for a deeper understanding of mechanisms that regulate the immune environment and response to treatment. Here, an integrative, multi-omic approach was employed to characterize DLBCL immune environments, which effectively segregated DLBCLs into four quadrants – termed DLBCL-immune quadrants (IQ) - defined by cell-of-origin and immune-related gene set expression scores. Recurrent genomic alterations were enriched in each IQ, suggesting that lymphoma cell-intrinsic alterations contribute to orchestrating unique DLBCL immune environments. In relapsed/refractory DLBCL patients, DLBCL-IQ assignment correlated significantly with clinical benefit with the CD20 x CD3 BsAb, mosunetuzumab, but not with CD19-directed CAR T cells. DLBCL-IQ provides a new framework to conceptualize the DLBCL immune landscape and uncovers the differential impact of the endogenous immune environment on outcomes to BsAb and CAR T cell treatment.

60 **Introduction**

61 Immunotherapies such as chimeric antigen receptor (CAR) T cell therapy and bispecific
62 antibodies (BsAbs) have revolutionized the treatment landscape of relapsed or refractory (r/r)
63 diffuse large B cell lymphoma (DLBCL). For example, CD19-directed CAR T cell therapy induces
64 durable responses in ~30-40% of patients with r/r DLBCL (1–4). Complete responses are also
65 observed in up to 40% of r/r DLBCL patients who receive CD20 x CD3 BsAbs (5–7). However,
66 in many r/r DLBCL patients, BsAbs and CAR T cell therapy either fail completely or confer only
67 fleeting responses. Collectively, these clinical observations indicate that while immunotherapies
68 can be effective against DLBCL, additional research is needed to understand the cellular and
69 molecular features of the DLBCL environment that underlie immunotherapy responsiveness or
70 resistance to enrich for the subset of patients who will derive maximal benefit and to identify
71 strategies to overcome mechanisms driving intrinsic or acquired resistance.

72 Numerous studies have demonstrated that a "T cell-inflamed" environment identifies solid
73 cancers against which a spontaneous anti-tumor immune response has been raised and serves as a
74 useful biomarker of response to checkpoint blockade therapy (CBT) (8–11). Transcriptional and
75 immune cell profiling of DLBCL has also revealed subsets enriched in immune cell infiltration
76 and in expression of immune-related genes, which indicates that some DLBCLs exhibit evidence
77 of having stimulated an endogenous anti-lymphoma immune response (12–15). However, the
78 critical factors that shape the DLBCL immune environment are unclear and the impact of the
79 immune environment on promoting or preventing immunotherapy response has yet to be fully
80 defined (16,17). Therefore, in this study, we utilized an integrative approach to 1) broadly
81 characterize the DLBCL immune landscape, 2) provide insight into the contribution of genomic
82 alterations in shaping the DLBCL immune environment, and 3) define the extent to which

transcriptionally based immune clustering of DLBCL informs responsiveness to CD20 x CD3 BsAb and CAR T cell immunotherapy. Through these analyses, we uncovered four unique DLBCL immune environments (or immune quadrants - IQs), each enriched for several distinct oncogenic alterations, suggesting that lymphoma cell-intrinsic factors play an important role in orchestrating the immune environment in this disease. For example, we identified loss-of-function (LoF) mutations in *SOCS1* as significantly enriched in DLBCLs with inflamed environments, and that genetic ablation of *Socs1* renders B cells more sensitive to the effects of T cell effector cytokines such as interferon-gamma (IFNγ). Finally, we find that DLBCL-IQ assignment impacts clinical outcomes to BsAb but not CAR T cell treatment, which suggests a differential effect of the endogenous immune environment on DLBCL outcomes to these two immunotherapy treatments.

106 ## Results

107 **Transcriptomic analysis identifies four immune-related DLBCL clusters.**

108 In solid cancers, a "T cell inflamed" gene signature identifies tumors against which a
109 spontaneous anti-tumor immune response has been induced and enriches for a subset of cancers
110 that are particularly vulnerable to immunotherapies, such as CBT (8–11). To determine if DLBCLs
111 could be similarly segregated, we performed bulk transcriptional analyses focused specifically on
112 immunological aspects of the lymphoma environment. Our discovery cohort consisted of
113 transcriptomic data from diagnostic DLBCL biopsies from the National Cancer Institute (NCI, n
114 = 481) (18,19) and an internal dataset from the University of Chicago Medical Center (UCMC, n
115 = 96) (20), comprising a total of 577 cases (*See Methods for details)*.

116 Gene set variation analysis (GSVA) (21) was used to calculate sample-wise relative
117 enrichment scores for 19 gene sets that fell into 2 functional groups: 1) twelve immune-related
118 signatures that reflect the presence or activation state of immune cell subsets, and 2) seven cell-of-
119 origin (COO) - related signatures **(Supplementary Table 1)**. Immune-related signatures were
120 manually curated from an extensive literature search and contained gene sets related to: IFNγ
121 response (8), type I IFN response (11), $CD8^+$ T cell activation (11,22,23) and exhaustion (11), T
122 helper subsets ($T_h1$ (22), $T_h2$ (22), T follicular helper ($T_{fh}$) (22), and regulatory T cells ($T_{reg}$) (11)),
123 macrophages (11), and dendritic cells (24). As COO segregates DLBCLs into activated B-cell-like
124 (ABC) and germinal center B-cell-like (GCB) subtypes with distinct clinical, transcriptional, and
125 genetic features, we hypothesized that COO would also significantly influence the composition of
126 the DLBCL immune environment. Therefore, we included gene sets derived from a validated gene
127 expression-based COO classifier (25), as well as gene sets regulated by IRF4 (26) and BCL6 (26),

128 transcription factors critical for COO classification. Altogether, 577 unique genes were included
129 in the 19 gene sets selected for GSVA (< 15% overlap between individual gene sets).

130 GSVA scores for the 577 DLBCLs in the discovery cohort were next subjected to principal
131 component analysis (PCA), which revealed that the majority (69.8%) of variance in gene set
132 expression scores was explained by PC1 (45.38%) and PC2 (24.43%). Unsupervised k-means
133 clustering performed on the PCA-transformed dataset revealed that the optimal number of clusters
134 was four **(Supplementary Figure 1A)**. DLBCLs in our discovery cohort were then assigned to
135 one of four specific clusters described below. Samples from NCI and UCMC datasets were equally
136 represented in each cluster, indicating the absence of significant batch effects **(Supplementary**
137 **Figure 1B and C)**.

138 Individual immune-related gene set expression scores were highly correlated, trending in
139 the same direction along PC1 **(Figure 1A)** and made minimal contributions to PC2
140 **(Supplementary Figure 1D and E)**, indicating that PC1 represented an immune-related axis. In
141 support of this notion, differential gene expression (DGE) analysis of putative "hot" DLBCLs
142 (PC1 > 0) and "cold" DLBCLs (PC1 < 0) revealed upregulation of genes linked to immune cell
143 infiltration and activation (*CD2, CD3D, GZMK, IFNG, CD8A, PRF1*) in the former
144 **(Supplementary Figure 1F)**. ABC COO-related gene sets (ABCDLBCL-1, ABCDLBCL-2,
145 IRF4Up-7) were highly correlated and positively associated with PC2, while GCB COO-related
146 gene sets (GCBDLBCL-1, GCBDLBCL-2, IRF4Dn-1) were negatively associated with PC2,
147 indicating that PC2 represented a COO-related axis **(Figure 1A, Supplementary Figure 1D and**
148 **E)**. Comparative analysis of the transcriptomes of putative "ABC" DLBCLs (PC2 > 0) and "GCB"
149 DLBCLs (PC2 < 0) identified several genes known to drive COO classification **(Supplementary**
150 **Figure 1G)**. Orthogonal validation demonstrated that GSVA-defined "ABC" (PC2 > 0) and

151 “GCB” (PC2 < 0) DLBCLs exhibited >95% concordance with COO designations from established
152 COO classifiers, confirming our GSVA was accurately classifying DLBCLs based on COO
153 **(Figure 1B and C)** (15,25). Thus, immune-related and COO-related gene sets are orthogonal and
154 segregate DLBCLs into 4 quadrants based on a distinct distribution of immune-related (PC1) and
155 COO-related (PC2) scores, referred to as DLBCL-immune quadrants (DLBCL-IQ). Specifically,
156 ABC DLBCLs could be transcriptionally defined as “ABC hot” (n = 182, 31.5%, PC1 > 0, PC2 >
157 0), characterized by high enrichment scores for ABC COO-related and immune-related gene sets,
158 or “ABC cold” (n = 184, 31.9%, PC1 < 0, PC2 > 0). Similarly, GCB DLBCLs could be subdivided
159 into “GCB hot” (n =122, 21.1%, PC1 > 0, PC2 < 0) and “GCB cold” (n = 89, 15.4%, PC1 < 0,
160 PC2 < 0) clusters **(Figure 1D and E)**.

161 When an identical GSVA was performed on an independent DLBCL dataset (British
162 Columbia Cancer, BCC, n = 285) (27,28), a similar clustering pattern emerged **(Supplementary**
163 **Figure 2A)**, with immune-related gene sets contributing to PC1 and COO-related gene sets
164 contributing to PC2 **(Supplementary Figure 2B)**. Therefore, the NCI/UCMC and BCC datasets
165 were combined to power downstream analyses. In the combined dataset (n = 862), DLBCLs from
166 different sources (NCI/UCMC versus BCC) were similarly distributed among each of the four IQs
167 **(Supplementary Figure 2C and D)** indicating an absence of batch effect. Moreover, the
168 combined dataset was again distributed into four distinct IQs, demonstrating the stability of
169 GSVA-based clustering in classifying DLBCLs by COO and their immune environment
170 **(Supplementary Figure 2E and F)**.

171

172 **Validation of transcriptionally defined DLBCL-IQs.**

173 Next, to confirm that DLBCL-IQs accurately reflect the actual immune cell composition
174 of specific lymphoma environments, multispectral immunofluorescence (mIF) was performed on
175 a subset of DLBCLs (n = 65, UCMC) for which paired RNA-seq data were available. Staining was
176 performed using fluorescently labeled antibodies against T cell markers (CD4 and CD8),
177 macrophage markers (CD68), DAPI, and B cells (PAX5). Macrophage ($CD68^+$) to DLBCL
178 ($PAX5^+$) cell ratios were similar across immune clusters **(Supplementary Figure 3A)** and were
179 not significantly correlated with sample-wise hot/cold (PC1) axis scores **(Supplementary Figure**
180 **3B)**. However, there were significant differences in T cell infiltration among the four DLBCL-
181 IQs. Representative images of a hot and cold DLBCL are shown in **Figure 2A**. DLBCLs
182 transcriptionally clustered by GSVA as ABC or GCB hot were characterized by significantly
183 higher ratios of $CD8^+$ T cells to DLBCL cells when compared to ABC and GCB cold counterparts
184 **(Figure 2B)**. Furthermore, $CD8^+$ T cell to DLBCL cell ratios were significantly correlated with
185 sample-wise hot/cold (PC1) axis scores **(Figure 2C)**. The same was true for $CD4^+$ T cell to DLBCL
186 cell ratios (**Figure 2D and E**). These data validate the accuracy of GSVA-based clustering in
187 classifying DLBCLs as harboring hot or cold immune environments.
188
189 **Prognostic significance of DLBCL-IQs.**
190 Next, the extent to which our DLBCL-IQs correlated with clinical outcomes to initial
191 treatment with R-CHOP was assessed. As expected, DLBCLs assigned to GCB clusters showed
192 improved progression-free survival (PFS) and overall survival (OS) compared to DLBCLs
193 assigned to ABC clusters. However, further stratifying within ABC or GCB clusters according to
194 hot or cold IQ assignment did not impact survival outcomes. **(Supplementary Figure 4A and**
195 **B).**

196 **Concordance of DLBCL-IQs with other immune-related DLBCL subtypes.**

197 Recently, DLBCLs have been classified according to the composition of their immune
198 environments. For example, Kotlov and colleagues recently classified DLBCLs into four
199 lymphoma microenvironments (LMEs) based on functional gene expression signatures ($F^{GES}$) that
200 reflected the relative abundance and functional features of cellular constituents (15). When LME
201 cluster annotations were applied to DLBCLs in our combined NCI/UCMC/BCC dataset, we found
202 that DLBCLs assigned to the ABC hot cluster overlapped significantly with an inflammatory
203 microenvironment (LME-IN) **(Supplementary Figure 5A)**. GCB and ABC cold DLBCLs were
204 equally represented within the depleted environment (LME-DE) **(Supplementary Figure 5A)**.
205 Finally, germinal center-like (LME-GC) and mesenchymal (LME-ME) did not overlap
206 significantly with any GSVA-defined immune clusters **(Supplementary Figure 5A)**.

207 Additionally, Steen et al. have introduced Ecotyper, a molecular classifier that integrates
208 immune cell deconvolution with single-cell RNA sequencing to characterize diverse DLBCL cell
209 states and ecosystems within the DLBCL environment. When comparing the overlap between our
210 DLBCL-IQs and the 9 lymphoma ecotypes (LE), we noted that approximately 65% of DLBCLs
211 in the ABC cold cluster were classified into LE1 and LE2, which are distinguished by the highest
212 expression of ABC COO-related genes and the greatest abundance of B cells, while being deficient
213 in T cell subsets **(Supplementary Figure 5B)**. Similarly, around 55% of GCB cold DLBCLs were
214 assigned to LE8, which is marked by an increased abundance of B cells and the expression of
215 GCB-associated genes **(Supplementary Figure 5B)**. Notably, DLBCLs in the LE8 cluster
216 exhibited significant overlap with $DZsig^{+}$ DLBCLs. Finally, LE4, characterized by enrichment in
217 ABC-related genes and an abundance of $CD4^{+}$ T cells, $CD8^{+}$ T cells, NK cells, and Tregs,
218 predominantly consisted of ABC hot DLBCLs. Minimal overlap was observed between the

219 remaining LEs and our GSVA-based IQs. Collectively, these results suggest LME and Ecotyper
220 capture different aspects of the lymphoma microenvironment and only partially overlap with our
221 DLBCL-IQs.
222
223 **Genomic features associated with DLBCL-IQs.**
224 Emerging evidence indicates that specific oncogenic alterations and associated
225 transcriptional programs can significantly impact the composition of the tumor immune
226 environment and vulnerability to immunotherapies in solid tumors (29–37). Therefore, we
227 analyzed paired whole exome sequencing (WES) and copy number alterations (CNA) for DLBCLs
228 in the combined cohort to identify genetic features associated with each of our GSVA-based
229 DLBCL-IQs.
230 In DLBCL, several landmark studies have developed genomic approaches to describe new
231 DLBCL subtypes based on the presence of specific co-occurring genetic alterations, including a
232 probabilistic classifier called LymphGen (18,38,39). However, the association of specific
233 LymphGen clusters with distinct immune environments has not been fully elucidated. LymphGen
234 cluster annotations were available for 754 DLBCLs in our combined dataset. Broadly speaking,
235 LymphGen classifications overlapped imperfectly with our DLBCL-IQs **(Figure 3A)**, with a few
236 notable exceptions. For example, DLBCLs characterized by activating *NOTCH1* mutations
237 (LymphGen N1 subtype), were significantly enriched in the ABC hot cluster, while DLBCLs with
238 *TP53* loss and aneuploidy (LymphGen A53 subtype), were almost exclusively found in the ABC
239 cold cluster. Lastly, DLBCLs with gain-of-function mutations in *EZH2*, *BCL2* translocations, and
240 *MYC* activation (LymphGen EZB-MYC$^{+}$ subtype), were enriched in the GCB cold cluster. The
241 remaining four LymphGen subtypes showed little correlation with specific GSVA-based immune-

242 related clusters, and LymphGen unclassified DLBCLs (~40% of all DLBCLs) were broadly
243 distributed among all four IQs **(Figure 3A)**.

244 To examine whether individual mutations or CNAs were associated with particular
245 DLBCL-IQs, we compared the genetic landscapes of DLBCLs assigned to each of the four
246 DLBCL-IQs (n = 842). The analysis was restricted to 190 essential driver genes to identify those
247 most relevant to DLBCL biology **(Supplementary Table 2)** (38,40). Comparative analysis of hot
248 DLBCLs versus cold DLBCLs (as defined by PC1) independent of COO identified several genetic
249 lesions associated with cold immune environments, including *FOXO1*, *MYD88,* and *TMEM30A*.
250 Fewer genetic alterations were significantly enriched in hot DLBCLs, but included alterations in
251 *SOCS1*, *TNFRSF14,* and *CD274* **(Supplementary Figure 6A)**. As ABC and GCB DLBCLs arise
252 in the context of distinct genetic alterations and oncogenic pathways, we next compared oncogenic
253 alterations specifically enriched in ABC hot versus ABC cold DLBCLs, and GCB hot versus GCB
254 cold DLBCLs. Alterations in genes such as *MYD88, KLHL14, CARD11,* and *TMEM30A,* known
255 to be potent drivers of chronic BCR signaling, were strongly enriched in ABC cold DLBCLs (41–
256 43) **(Figure 3B)**. Alterations in *CD274* (*PD-L1*) were significantly enriched among ABC hot
257 DLBCLs **(Figure 3B)**, concordant with our previous work (20). Mutations in *RB1*, *FOXO1*, and
258 *GNA13* were enriched in the GCB cold cluster, while those in *TNFAIP3* and *SOCS1* were
259 significantly associated with the GCB hot cluster **(Figure 3C)**.

260 To gain insight into the impact of oncogenic signaling pathways on DLBCL immune
261 environments, mutations and CNAs were grouped into functional pathways. Notably, genetic
262 alterations in the BCR-dependent NF-κB signaling pathway were significantly enriched in ABC
263 cold DLBCLs compared to ABC hot DLBCLs **(Supplementary Figure 6B)** (43,44). ABC and
264 GCB cold DLBCLs were both significantly enriched for alterations in genes involved in p53

265 signaling and cell cycle progression compared to ABC and GCB hot DLBCLs, respectively
266 **(Supplementary Figure 6C)** (45).

267 Finally, gene set enrichment analysis (GSEA) showed upregulation of immune-related
268 gene sets, including IFNγ targets, IFNα response genes, and IL2-STAT5 signaling pathway genes
269 in ABC hot and GCB hot clusters (**Figure 3D**). In contrast, G2M target gene sets were enriched in
270 ABC and GCB cold DLBCL clusters, suggesting dysregulated lymphoma cell cycling might play
271 a role in orchestrating cold DLBCL immune environments **(Figure 3D and E)**. GSEA also
272 demonstrated that ABC and GCB cold DLBCLs were significantly enriched for expression of
273 MYC target genes compared to ABC and GCB hot DLBCLs (**Figure 3D and F**). Taken together,
274 these data show that several genetic lesions and oncogenic pathways are recurrently associated
275 with specific GSVA-defined DLBCL-IQs, suggesting that lymphoma cell-intrinsic alterations may
276 impact the immune environment in DLBCL.

277

278 **MYC activation is strongly associated with cold DLBCL immune environments.**

279 Because GSEA showed striking upregulation of MYC targets in cold DLBCLs, the role of
280 MYC in orchestrating a cold immune environment was further interrogated. We devised a MYC
281 GSVA score using genes from a previously published target gene signature (MycUp-4) to assign
282 DLBCLs into "MYC-High," "MYC-Low", or "MYC-Int" groups (46). IHC for MYC expression
283 was performed on DLBCLs in the BCC cohort with paired transcriptomic data (n = 266). DLBCLs
284 with high MYC protein expression – defined as ≥ 40% of lymphoma cells expressing MYC by
285 IHC staining – were consistently classified as MYC-high transcriptionally (MYC-High).
286 Conversely, DLBCLs identified as MYC-Low transcriptionally were characterized by low MYC

287 protein expression. Thus, expression of the transcriptional MYC signature accurately identifies
288 DLBCLs with high versus low MYC protein expression **(Supplementary Figure 7A)**.
289 ABC cold and GCB cold DLBCLs showed significantly higher expression of the MYC
290 activation signature compared to ABC hot or GCB hot DLBCLs **(Supplementary Figure 7B)** and
291 MYC-High DLBCLs were equally distributed between ABC cold (40%) and GCB cold (40%)
292 clusters **(Supplementary Figure 7C)**. Compared to their MYC-Low counterparts, MYC-High
293 DLBCLs in both ABC and GCB clusters contained significantly lower inferred proportions of
294 immune cell subsets when analyzed by CIBERSORTx **(Supplementary Figure 7D-F)**, suggesting
295 a negative correlation between MYC activation and an inflamed environment (47). Supporting this
296 notion, DLBCLs in the MYC-High group were characterized by lower $CD8^+$ T cell to DLBCL cell
297 ratios compared to MYC-Low DLBCLs when assessed by mIF **(Supplementary Figure 7G)**.
298 $CD8^+$ T cell to DLBCL cell ratios were also negatively correlated with a sample wise MYC GSVA
299 score **(Supplementary Figure 7H)**. Similar findings were also observed for $CD4^+$ T cells
300 **(Supplementary Figure 7I and J)**. Taken together, these data reveal a strong association between
301 MYC activity and cold immune environments in DLBCL.
302
303 ***SOCS1* mutations are enriched among GCB hot DLBCLs and enhance B-cell sensitivity to**
304 **IFNγ.**
305 We were particularly intrigued by the strong association between GCB hot DLBCLs and
306 putative LoF *SOCS1* mutations as SOCS1 is also frequently mutated in classical Hodgkin
307 lymphoma (cHL) (48–50) and primary mediastinal B cell lymphoma (PMBL) (48,51–53) – two
308 lymphoma subtypes associated with inflamed immune environments and remarkable sensitivity to
309 CBT (16,17,54–57). SOCS1 is a tumor suppressor and potent negative regulator of JAK/STAT

310 signaling, and LoF mutations in *SOCS1* have been implicated in enhancing oncogenic JAK/STAT
311 signaling in lymphoma downstream of cytokines such as IL-4 and IL-13 (58–62). However, as
312 critical T cell effector cytokines such as IFNγ also signal through the JAK/STAT pathway, we
313 hypothesized that LoF *SOCS1* mutations may render DLBCLs more sensitive to the effects of
314 IFNγ, which could stimulate the generation of "inflamed" environments (63–65).

315 *SOCS1* LoF alterations were identified in 16.2% of DLBCLs in our combined cohort and
316 were significantly associated with a GCB COO **(Figure 4A**). As expected, the incidence of *SOCS1*
317 mutations was significantly higher in the GCB hot cluster (30.3%) compared to other IQs **(Figure**
318 **4A and B)**. *SOCS1* mutations were often missense or nonsense (82.3%) and occurred with similar
319 frequencies across the *SOCS1* gene **(Figure 4B),** consistent with the role of SOCS1 as a tumor
320 suppressor. Immune cell deconvolution revealed an increased inferred fraction of several immune
321 cell subsets, including $CD8^+$ T cells and $CD4^+$ T cells, in *SOCS1* mutant compared to *SOCS1*
322 wildtype GCB DLBCLs suggesting that GCB DLBCLs with *SOCS1* mutations are more inflamed
323 than their *SOCS1* wildtype counterparts **(Figure 4C)**. Moreover, among GCB DLBCLs, GSEA
324 demonstrated increased expression of IFNγ and IFNα signaling pathway associated genes in
325 *SOCS1* mutant DLBCLs compared to *SOCS1* WT DLBCLs **(Figure 4D)**.

326 To directly test the hypothesis that loss of Socs1 function would render B cells more
327 sensitive to IFNγ, splenocytes from *Socs1*-deficient ($Cd19^{Cre/+}Socs1^{fl/fl}$) or *Socs1*-sufficient mice
328 ($Cd19^{Cre/+}$) were subjected to IFNγ stimulation. Representative gating of $CD19^+$ B cells and $CD3^+$
329 T cells is shown in **Supplementary Figure 8A**. As hypothesized, IFNγ response genes, such as
330 MHC-II, and PD-L1, were significantly more inducible by IFNγ in a dose-dependent manner in
331 splenic $CD19^+$ B cells from mice lacking *Socs1* compared to wildtype controls **(Figure 4E,**
332 **Supplementary Figure 8B)**. This effect was specific to $CD19^+$ cells in which *Socs1* had been

333 deleted, as MHC-II and PD-L1 were similarly inducible in $CD3^+$ T cells isolated from spleens of
334 conditional *Socs1*-sufficient and *Socs1*-deficient mice **(Supplementary Figure 8C)**. These data
335 demonstrate that DLBCLs with *SOCS1* mutations represent a novel subset of inflamed lymphomas
336 that may be particularly vulnerable to T cell-based immunotherapies due to enhanced IFNγ
337 sensitivity.
338
339 **DLBCL-IQs are associated with distinct survival outcomes to BsAb therapy but not CAR T**
340 **cell treatment.**
341 The presence of activated T cells in the tumor environment has been associated with
342 response to CBT in solid cancers (8–11,66,67). However, the extent to which the local immune
343 environment impacts the effectiveness of immunotherapies, such as BsAbs and CAR T cells, has
344 not been well characterized in DLBCL. Therefore, we sought to define the degree to which our
345 DLBCL-IQs correlated with clinical benefit following treatment with mosunetuzumab, a CD20 x
346 CD3 BsAb and axicabtagene ciloleucel (axi-cel) CD19 CAR T cell therapy.
347 First, using the immune- and COO-related gene sets detailed earlier, GSVA was performed
348 on the transcriptomes of DLBCLs in our merged dataset (NCI/UCMC/BCC), along with pre-
349 treatment r/r DLBCL biopsies (n = 74) from patients enrolled in a phase I/II dose-escalation trial
350 of mosunetuzumab (5). Consistent with observations in our training and validation datasets, PCA
351 again revealed that PC1 reflected an immune-related axis and PC2 reflected a COO-related axis,
352 and segregated DLBCLs into four quadrants **(Figure 5A and B).** Next, we addressed the extent
353 to which GSVA-defined DLBCL-IQs were associated with differential outcomes to
354 mosunetuzumab treatment. Independent of COO, r/r DLBCLs characterized as "hot" (n = 32)
355 demonstrated significantly improved PFS with mosunetuzumab treatment (HR = 0.58 (0.34-0.97)

356 , p = 0.038) compared to those classified as "cold" (n = 42) **(Figure 5C)**. Outcomes to
357 mosunetuzumab treatment were next compared between ABC hot and ABC cold, as well as GCB
358 hot and GCB cold DLBCLs. Interestingly, patients with GCB hot DLBCLs demonstrated
359 significantly improved PFS compared to those with GCB cold DLBCLs (HR = 0.35 (0.14-0.85),
360 p = 0.02) **(Figure 5D).** Patients with GCB cold DLBCLs demonstrated extremely poor outcomes
361 after treatment with mosunetuzumab, with a median PFS of only 2.3 months. Conversely, PFS
362 following mosunetuzumab treatment was similar among patients with ABC hot and ABC cold
363 DLBCLs, indicating that the pre-treatment immune environment can significantly influence
364 response to mosunetuzumab immunotherapy in patients with r/r GCB DLBCL (**Supplementary**
365 **Figure 9A)**.

366 As DLBCL-IQs were associated with differential clinical benefit with mosunetuzumab, we
367 hypothesized this might also be the case for other T cell-based immunotherapies, such as CAR T
368 cell therapy. Therefore, we performed GSVA on pre-treatment biopsies of DLBCL patients treated
369 with axi-cel (n = 51) combined with our merged dataset (NCI/BCC/UCMC) (68). Similar to our
370 previous results, DLBCLs were distributed along an immune-related axis (PC1) and COO-related
371 axis (PC2) into four equally sized IQs **(Supplementary Figure 9B and Figure 5E)**. However, in
372 contrast to patients treated with mosunetuzumab, patients with "hot" DLBCLs (n = 33, PC1 > 0)
373 had similar event free survival (EFS) and OS as those with "cold" DLBCLs (n = 40, PC1 < 0)
374 following CAR T cell treatment **(Supplementary Figure 9C and D)**. Moreover, specific DLBCL-
375 IQs were not significantly associated with improved EFS or OS with CAR T cell therapy, although
376 DLBCLs classified as GCB hot trended towards improved EFS **(Figure 5F and Supplementary**
377 **Figure 9E)**. Taken together, these data suggest that the DLBCL immune environment is correlated

378 with benefit to BsAbs but not CAR T cell therapy, indicating that the mechanism and extent to
379 which these immunotherapies rely on the endogenous immune environment may differ.
380

381 **Discussion**

382 Previous transcriptional analyses have demonstrated significant heterogeneity in the
383 immune landscapes of DLBCL (12,15,68). Yet, the precise mechanisms governing these distinct
384 immune environments and their potential association with the response to immunotherapy in
385 DLBCL remain largely unexplored. Here, we curated immune- and COO-related gene sets and
386 performed GSVA to analyze bulk transcriptomes of 862 diagnostic DLBCL samples across three
387 large datasets, which effectively segregated DLBCLs into four IQs: GCB cold, GCB hot, ABC
388 cold, and ABC hot. Importantly, we identified strong associations between recurrent genetic
389 alterations and each GSVA-defined IQ, which suggests that tumor cell-intrinsic alterations have a
390 significant impact in regulating the immune landscape of DLBCL. Finally, we uncovered a striking
391 relationship between the pre-existing immune landscape and response to CD20 x CD3 BsAb
392 treatment, but not CAR T cell therapy, in patients with r/r DLBCL.

393 Interestingly, our data indicate that classifying DLBCLs along an immune axis (PC1) score
394 can accurately identify "inflamed" DLBCLs that exhibit improved PFS to treatment with the CD20
395 BsAb, mosunetuzumab. Surprisingly, we identified that COO significantly influences this
396 association, as only GCB hot DLBCLs exhibited improved PFS following mosunetuzumab
397 treatment. This finding suggests that for r/r GCB DLBCLs, the pre-existing immune environment
398 is clearly an important factor associated with benefit from BsAb immunotherapy. In contrast, the
399 PC1 axis was not associated with improved survival following treatment with axi-cel. These
400 findings align with a recent analysis of pre-treatment DLBCL biopsies from patients enrolled in

401 the ZUMA-7 study, where the expression of T cell-associated transcripts was not associated with
402 a significant EFS advantage after second-line axi-cel treatment (69). However, when considering
403 COO (PC2) in addition to PC1, we find that patients with GCB hot DLBCLs treated with axi-cel
404 also demonstrated a trend toward improved EFS compared to DLBCLs assigned to other DLBCL-
405 IQs similar to mosunetuzumab. Together, these data suggest that integrating COO and immune
406 signatures, as with DLBCL-IQ, may provide a more nuanced understanding of the factors that may
407 govern response or resistance to BsAb and CAR T cell therapy.

408 A central hypothesis underlying our analyses was that lymphoma cell-intrinsic alterations
409 significantly influence the composition of the DLBCL immune environment. Supporting this
410 notion, we found that each DLBCL-IQ was significantly enriched for distinct genetic lesions and
411 oncogenic pathways. For example, GCB hot DLBCLs were significantly enriched for *SOCS1* LoF
412 mutations, which are commonly observed in other inflamed lymphomas that are highly susceptible
413 to CBT, such as cHL and PMBL. Because *SOCS1* is a potent negative regulator of JAK/STAT
414 signaling, we hypothesized that LoF *SOCS1* mutations would sensitize B cells to IFNγ – a
415 JAK/STAT-dependent effector cytokine critical for effective anti-tumor immune responses
416 (8,9,61–63,70). Indeed, genetic alterations that blunt IFNγ sensing in tumors, such as LoF *JAK1/2*
417 alterations, lead to resistance to T cell-based immunotherapies (32,67,71–74). In contrast, loss of
418 negative regulators of IFNγ signaling, for example *PTPN2, PBRM1,* and *ARID2*, sensitize tumor
419 cells to IFNγ and T cell mediated cytolysis, are associated with inflamed tumor environments, and
420 have been linked with CBT responsiveness in solid tumors (34,35,75,76). Although the extent to
421 which LoF mutations in *SOCS1* directly mediate sensitivity to CBT in cHL and PMBL remains to
422 be elucidated, we find that genetic ablation of *Socs1* sensitizes murine B cells to IFNγ. Therefore,

423 these data suggest that *SOCS1* mutations identify a novel subset of "inflamed" DLBCLs that may
424 be inherently vulnerable to T cell-based immunotherapies that rely on this key effector cytokine.
425 Among ABC DLBCLs, mutations culminating in enhanced BCR activation, such as
426 *MYD88*$^{L265P}$*, CARD11, KLHL14*, and *TMEM30A* were significantly associated with cold immune
427 environments (26,44,77,78). The potential mechanism(s) by which oncogenic BCR signaling in
428 lymphoma cells leads to decreased T cell infiltration is unknown. However, we observed that ABC
429 cold DLBCLs exhibited higher MYC activity than GCB cold DLBCLs – a surprising finding since
430 MYC activity in GCB DLBCL is often driven by *MYC* translocations to the *IGH* locus, leading to
431 constitutive MYC expression (79–81). Therefore, we hypothesize that ABC DLBCL-associated
432 oncogenic pathways, namely BCR-dependent NF-κB signaling, may drive particularly potent
433 MYC activity and the acquisition of cold immune environments. This finding would have
434 significant translational relevance, as therapies that indirectly modulate MYC activity by acting
435 on BCR signaling may shift the balance toward a "hot" environment and sensitize DLBCLs to
436 immunotherapies.
437 While these results represent an important advance in our understanding of the DLBCL
438 immune environment, there are some limitations to our study. Firstly, GSVA assigns relative
439 enrichment scores, which might exhibit variability across datasets, thereby complicating
440 comparisons between different datasets. To address this limitation, we combined the
441 mosunetuzumab and Stanford CAR T cohorts with our merged dataset of DLBCLs
442 (NCI/BCC/UCMC), which may facilitate more direct comparisons between patients treated with
443 mosunetuzumab and axi-cel. Second, our analysis utilized bulk transcriptomic data from
444 diagnostic DLBCL samples, and it is unclear how prior therapies impact the immune landscape in
445 this disease. However, when we applied our GSVA-based clustering to the transcriptomes of two

446 independent cohorts of heavily pre-treated patients with r/r DLBCL, we identified a similar
447 distribution of immune-related scores, which preliminarily suggests a relatively limited effect of
448 cytotoxic therapy on the composition of DLBCL immune environments. Finally, the association
449 between particular DLBCL-IQs and clinical benefit from mosunetuzumab and CAR T cell therapy
450 was based on relatively small patient cohorts and the analyses were retrospective in nature. Despite
451 these limitations, our study provides valuable insights into the DLBCL immune environment and
452 its relevance to therapeutic responses, paving the way for further investigation and refinement of
453 treatment strategies in this complex disease.

454 In conclusion, our results demonstrate that genomic alterations in lymphoma cells can
455 impact the DLBCL immune environment. Furthermore, we show using DLBCL-IQ the differential
456 impact of the pre-treatment DLBCL immune environment on clinical benefit after BsAb versus
457 CAR T cell therapies. This latter observation is particularly important in suggesting that the
458 effectiveness of BsAbs might require a more "inflamed" microenvironment, whereas CAR T cells
459 may be efficacious even in "cold" DLBCLs. Finally, our data suggest that profiling the DLBCL
460 immune environment could be useful in delivering more personalized immunotherapy to r/r
461 DLBCL patients.

462

463

464

465

466

467

468

469 **Figures**

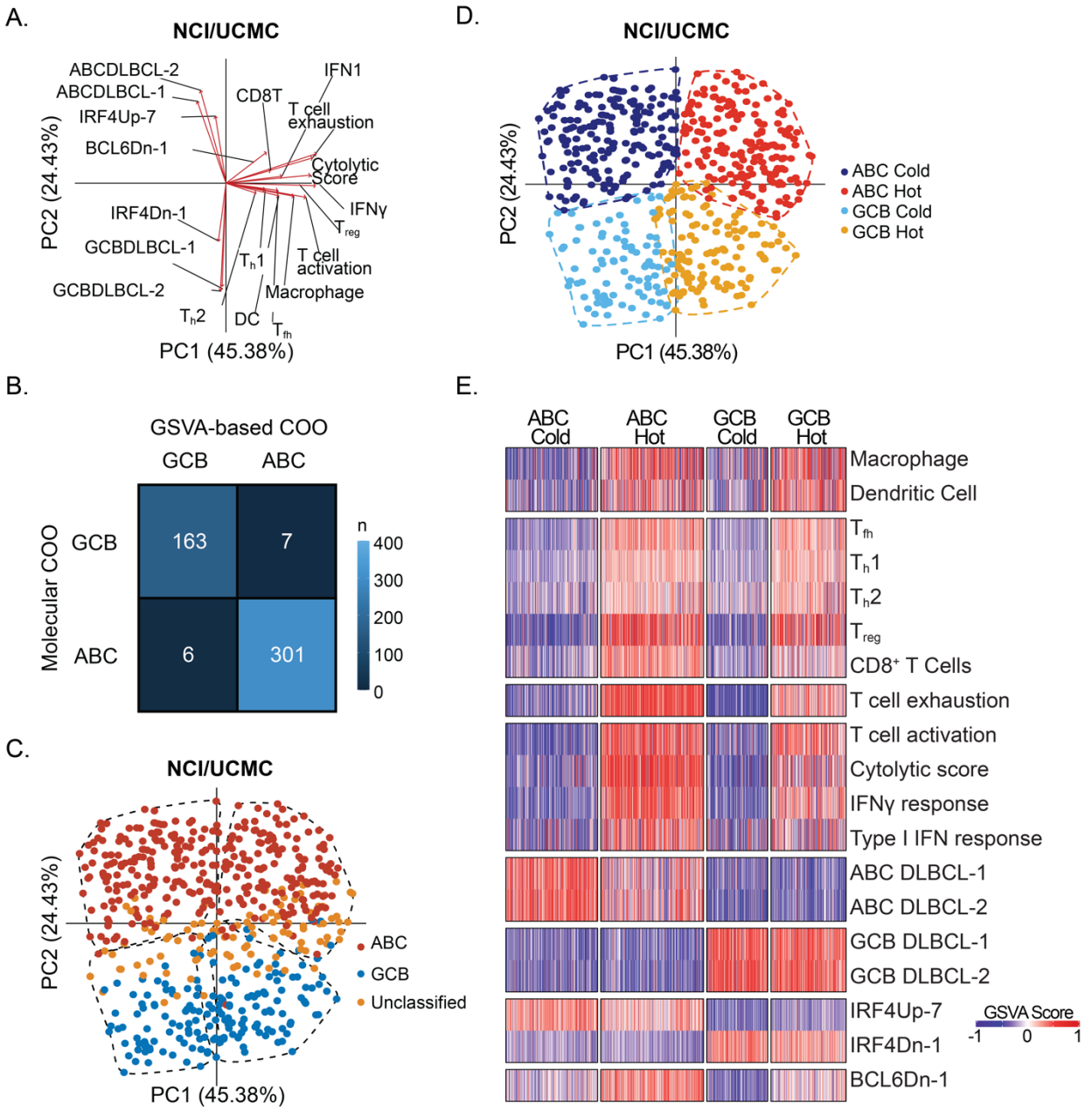


470 **Figure 1. Transcriptomic analysis identifies four unique DLBCL immune environments. A.**
471 Principal component analysis (PCA) biplot showing the contribution of immune-related gene sets
472 and COO-related gene sets to PC1 and PC2, respectively. **B**. Confusion matrix showing the
473 concordance between GSVA-based COO classification and molecularly defined COO

474 designations for all DLBCLs in the discovery cohort (NCI/UCMC, n = 577). **C.** PCA plot showing
475 concordance between sample-wise GSVA COO scores and molecularly defined COO calls for all
476 DLBCLs in the discovery cohort. Clusters are defined by the dashed line. **D.** PCA plot showing
477 sample-wise GSVA enrichment scores for DLBCLs in the discovery cohort, labeled by immune
478 quadrant (IQ) name (ABC Cold – dark blue, ABC Hot – red, GCB Cold – light blue, GCB Hot –
479 yellow). **E.** Heatmap showing sample-wise GSVA enrichment scores for all 19 gene sets.
480
481
482
483
484
485
486
487
488
489
490

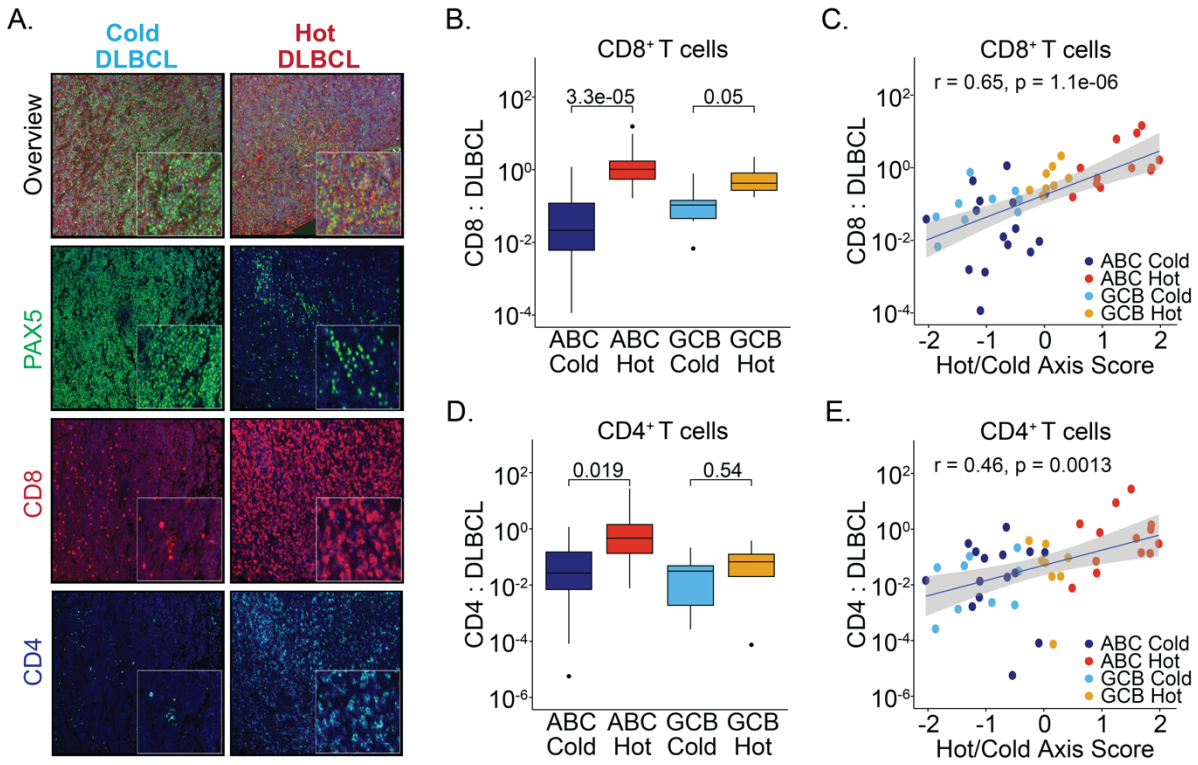


**Figure 2. Validation of transcriptionally defined DLBCL-IQs**. **A.** Representative multispectral immunofluorescence (mIF) images showing Pax5$^+$ lymphoma cells (green), CD8$^+$ T cells (red), CD4$^+$ T cells (blue) for a cold (left) and hot (right) DLBCL. **B.** Box plot showing average CD8$^+$ T cell : DLBCL cell ratios in immune-related clusters (n = 45). **C.** Scatter plot showing correlation of hot/cold axis score (PC1) and CD8$^+$ T cell : DLBCL cell ratio (n = 45). **D.** Box plot showing average CD4$^+$ T cell : DLBCL cell ratios in immune-related clusters (n = 45). **E.** Scatter plot showing correlation of hot/cold axis score (PC1) and CD4$^+$ T cell : DLBCL cell ratio (n = 45).

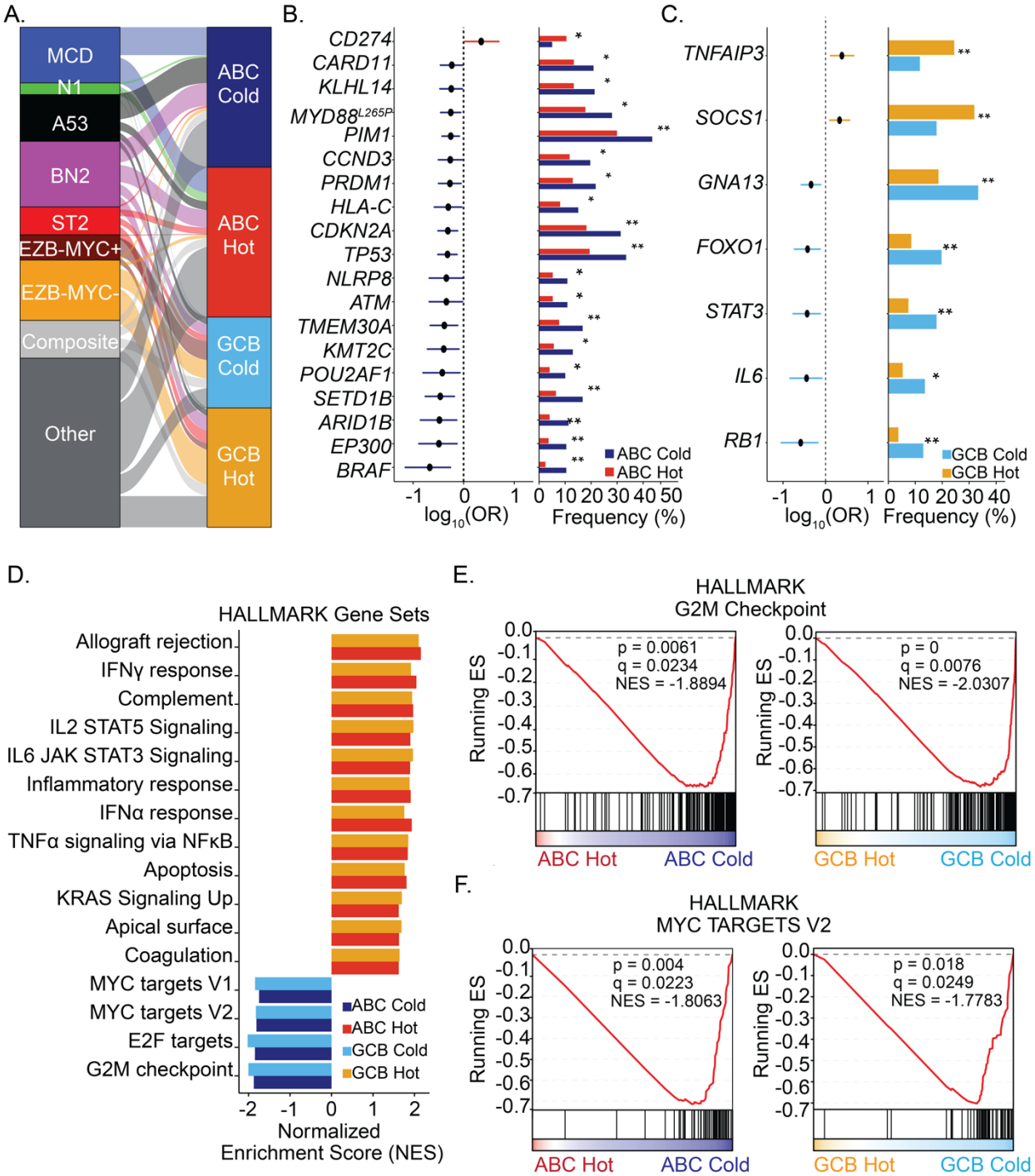


**Figure 3. Genomic features associated with DLBCL-IQs. A.** Alluvial plot showing overlap between LymphGen subtypes and DLBCL-IQs. **B.** Forest plot showing genetic alterations recurrently associated with ABC Hot or ABC Cold DLBCLs. **C.** Forest plot showing genetic

504 alterations recurrently associated with GCB Hot or GCB Cold DLBCLs. **D.** Bar plot of gene set
505 enrichment analysis (GSEA) showing gene sets significantly enriched in each immune-related
506 cluster. **E.** GSEA plots showing upregulation of G2M target gene sets in ABC cold and GCB cold
507 DLBCLs. **F.** GSEA plots showing upregulation of MYC checkpoint related genes in ABC cold
508 and GCB cold DLBCLs. OR – odds ratio; ES – enrichment score; NES – normalized enrichment
509 score. Fisher's exact test with BH-adjusted p values displayed. (* adj. $p < 0.1$, ** adj. $p < 0.05$,
510 *** adj. $p < 0.01$).
511

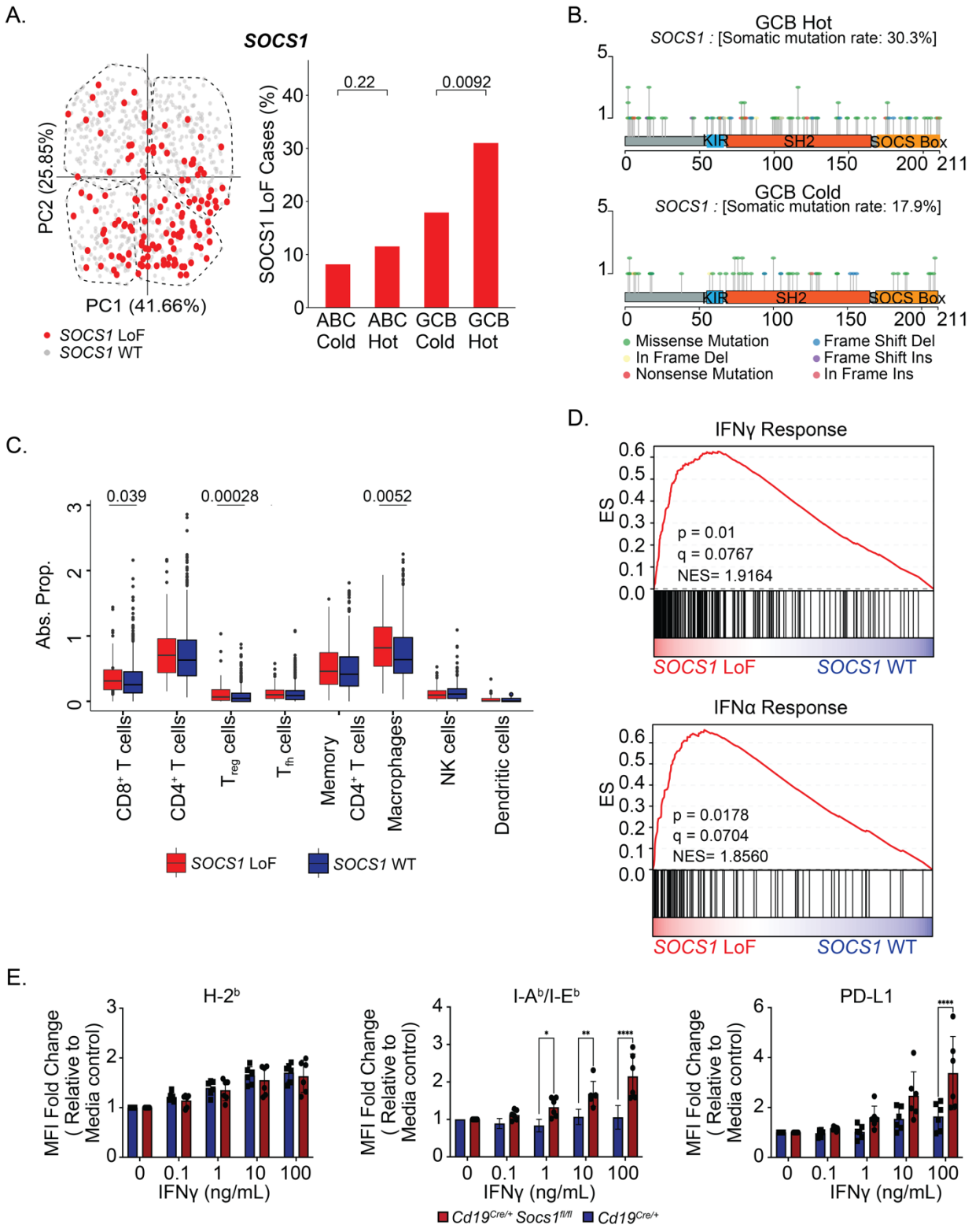


512

513 **Figure 4. *SOCS1* mutations are enriched among GCB Hot DLBCLs and enhance B-cell**

514 **sensitivity to IFNγ signaling. A.** PCA plot (left) and bar plot (right) showing the frequency of

515 *SOCS1* loss of function (LoF) alterations in each immune-related cluster. **B.** Lollipop plots
516 showing frequency and distribution of mutations in *SOCS1* in GCB Hot (top) and GCB cold
517 (bottom) DLBCLs. **C.** Immune cell deconvolution (CIBERSORTx) showing absolute inferred
518 proportions of indicated immune cell subsets in *SOCS1* LoF GCB DLBCLs compared to *SOCS1*
519 wildtype (WT) GCB DLBCLs. **D.** GSEA plots showing upregulation of IFNγ response genes and
520 IFNα response genes in *SOCS1* LoF GCB DLBCLs compared to *SOCS1* WT GCB DLBCLs.
521 Fisher's exact test with BH-adjusted p values for categorical variables. Kruskal-Wallis test
522 followed by post-hoc Dunn's test with adjusted p values for continuous variables. **E.** Fold change
523 in mean fluorescence intensity (MFI) of H-$2^b$, I-A/I-$E^b$, and PD-L1 on $CD19^+$ splenocytes. $CD19^+$
524 splenocytes from $Cd19^{Cre/+}$ (n = 6) or $Cd19^{Cre/+}$ $Socs1^{fl/fl}$ mice (n = 6) were cultured with media or
525 the indicated concentrations of IFNγ for 48 hours and expression levels of H-$2^b$, I-A/I-$E^b$, and PD-
526 L1 were measured. Mice were pooled from 3 independent biological replicates. Two-way
527 ANOVA with Bonferroni correction, adj. p values displayed (* adj. $p < 0.05$, ** adj. $p < 0.01$, ***
528 adj. $p < 0.001$, **** adj. $p < 0.0001$).

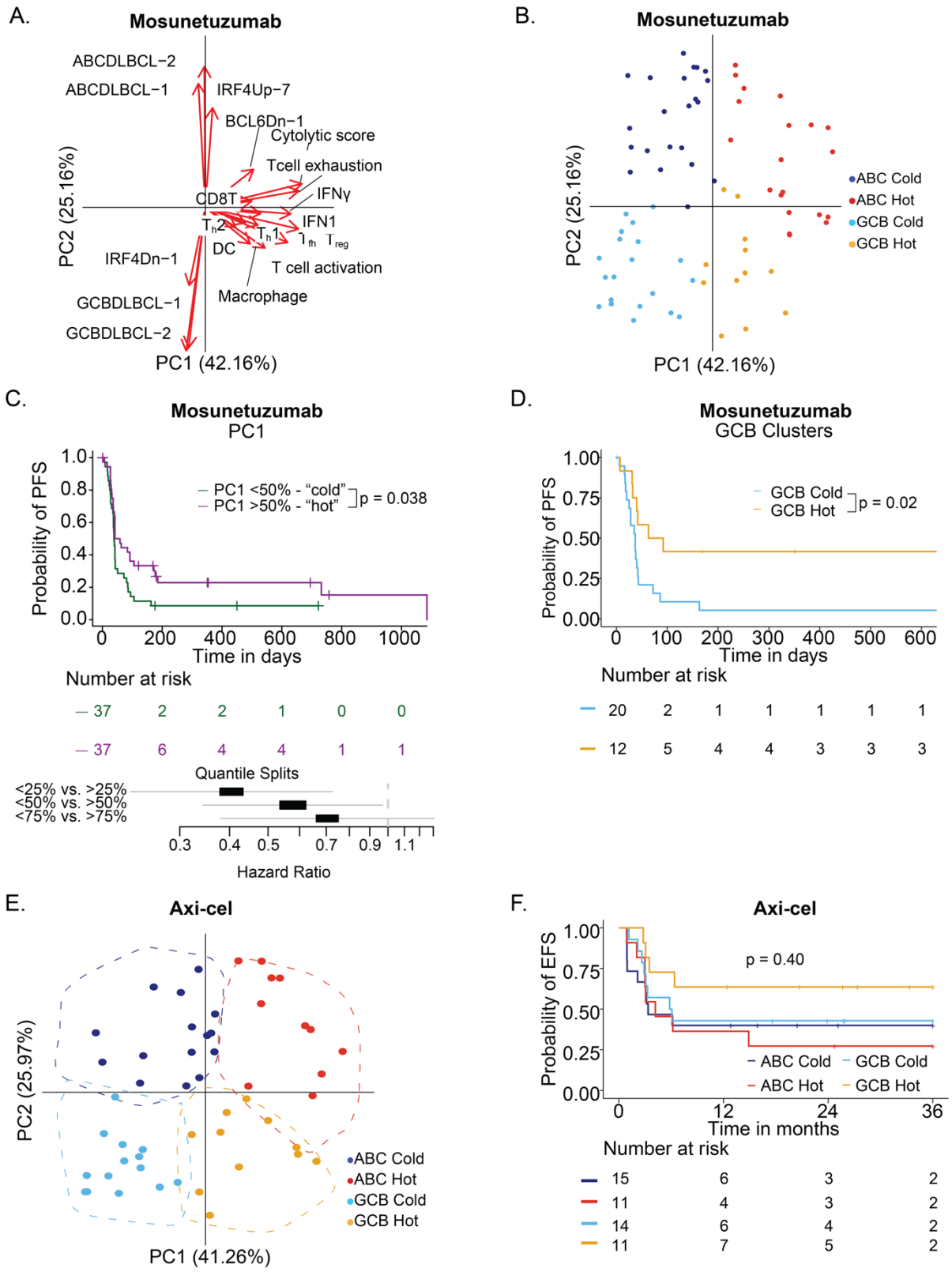


**Figure 5. DLBCL-IQs are associated with distinct survival outcomes to BsAb therapy but not CAR T cell treatment. A.** PCA biplot showing the contribution of immune-related gene sets

531 and COO-related gene sets to PC1 and PC2, respectively, for pre-treatment r/r DLBCL biopsies
532 (n = 74) from patients treated with mosunetuzumab. **B.** PCA plot showing sample-wise GSVA
533 enrichment scores for DLBCL biopsies from patients treated with mosunetuzumab. **C.** PFS for
534 patients assigned to "hot" or "cold" DLBCL immune clusters and treated with mosunetuzumab
535 (top) and forest plot showing hazard ratio of the association between PC1 score and PFS (bottom).
536 **D.** PFS for patients assigned to GCB Hot and GCB Cold DLBCL IQs and treated with
537 mosunetuzumab. Log-rank test with p value displayed. **E.** PCA plot showing sample-wise GSVA
538 enrichment scores for DLBCL biopsies from patients treated with axicabtagene ciloleucel (axi-
539 cel). **F.** Event free survival (EFS) for patients assigned to each DLBCL-IQ and treated with axi-
540 cel. Log-rank test with p value displayed.
541
542
543
544
545
546
547
548
549
550
551
552
553

554 # Methods

555 **Data sets**

556 ***NCI cohort***: RNA-sequencing counts for 481 DLBCL biopsies were downloaded from dbGaP
557 (phs001444) (18). All patients had variants calls from whole exome sequencing and copy number
558 arrays.

559 ***UCMC cohort***: RNA-sequencing was performed on 96 DLBCL biopsies (84 treatment-naïve, 12-
560 relapsed/refractory, 2 unknown). Paired whole exome sequencing was successful for 76 cases.

561 ***BCC cohort***: RNA-sequencing counts for 285 treatment-naive DLBCL biopsies was provided by
562 BCC (27,28). Of these, 283 patients had available variant calls from targeted sequencing and copy
563 number arrays.

564 ***Stanford cohort***: RNA-sequencing data quantified as transcripts per million (TPM) for 88 DLBCL
565 biopsies were downloaded from dbGaP (phs003145.v1.p1) (68).

566 Data were quantified as log2(TPM+1) for analysis.

567

568 **Molecular and genetic subtype classifications**

569 ***Cell of origin:*** COO classifications were compiled from previously described gene expression-
570 based classifiers. For the NCI cohort, all DLBCLs had COO calls from a DGE-based classifier
571 (25). For the BCC cohort, 283 DLBCLs had COO calls from Lymph3Cx (27). For the UCMC
572 cohort, all samples had COO calls from an RNAseq-based classifier from BostonGene (15).

573

574 ***LME classifications*****:** Lymphoma Microenvironment (LME) classifications for DLBCLs in the
575 NCI, BCC, and UCMC cohorts were provided by BostonGene (15).

576

577 ***Dark zone signature*:** DZsig (formerly known as double hit signature) classifications for the BCC
578 and NCI cohorts were obtained from Ennishi et al. (28) and Wright et al. (18), respectively. DZsig
579 classifications for the UCMC cohort were provided by BostonGene from an RNAseq-based
580 classifier (18).
581
582 ***LymphGen* classifications:** LymphGen classifications for the BCC and NCI cohorts were obtained
583 from Wright et al. (18).
584
585 **Generation and processing of sequencing data**
586 ***Quality control:*** FastQC and FastQ Screen were used to assess read quality and other species
587 contamination (www.bioinformatics.babraham.ac.uk). SNP (single nucleotide polyphorism)-
588 calling using pileup in FACETS was used to assess sample mix-ups and contamination (82).
589
590 ***Mutation-calling and annotation:*** Whole exome sequencing data for the UCMC cohort was
591 generated as previously described (20). Mutation-calling for whole exome sequencing data for the
592 UCMC cohort was performed similarly to the analysis in Kotlov et al (15). Reads were trimmed
593 using fastp to eliminate low-quality reads and then were aligned to the GRCh38 reference genome
594 using BWA (v0.7.17) (83,84). Duplicate reads were removed using Picard's MarkDuplicates
595 (v2.6.0) ("Picard Toolkit", 2019. Broad Institute, GitHub Repository) and recalibrated by
596 BaseRecalibrator and ApplyBQSR from GATK4 (85). For samples with a paired normal reference,
597 short variants were called using Strelka (86). For tumor-only samples, Pisces (v5.2) was used (87).
598 Variants were annotated using Variant Effect Predictor (VEP) (88). For all data sets, variants were
599 restricted to these predicted to be deleterious.

600 ***Copy number analysis:*** Copy number variation (CNV) was assessed using Sequenza with
601 modifications from FACETS (82,89). CNV analysis was performed in the space of genes listed in
602 **Supplementary Table 2.** Sequenza input reference was modified to match FACETS, calculated
603 using facets-pileup. For tumor-only samples, calling versus average normal or tumor sample was
604 performed using a modified version of Sequenza. Average normal/tumor pileup files were
605 prepared to average normalized coverage and variant allele fraction (VAF) at each position. Some
606 samples were excluded due to low coverage and/or tumor content. For all data sets, heterozygous
607 deletions and low-level copy gains were excluded.
608
609 ***RNA-seq processing and normalization:*** Paired-end and single-end RNA-seq data for the UCMC
610 cohort was generated as previously described (20). RNA-seq reads were aligned using kallisto
611 v0.42.4 to GENCODE v23 transcripts with default parameters (90). The protein-coding transcripts,
612 immunoglobulin heavy, kappa and lambda light chains, and TCR-related transcripts were retained;
613 noncoding RNA, histone, and mitochondria-related transcripts were removed. Counts were
614 processed using limma (v3.52.4) and edgeR (v3.38.4). Genes with low counts were removed using
615 a threshold of a 0.5 log2CPM average across all samples, as previously described (21). Then, TMM
616 (trimmed mean of M-values) normalization was performed, and counts were quantified as
617 log2CPM. Batch correction was performed using the removeBatchEffect function in limma.
618 For DLBCLs in the mosunetuzumab cohort, robust library sizes were estimated using DESeq2,
619 and raw RNASeq counts were normalized via limma-voom.
620
621 **Differential gene expression (DGE) and gene set enrichment analysis (GSEA)**:

622 DGE was performed using voom, and differentially expressed genes were generally defined as
623 those with |log2FC| ≥ 1 and adjusted p value < 0.05 (91). GSEA was performed using the Desktop
624 client (v4.2.3) with default settings (92).
625
626 **Comparing variants between groups**
627 Variants were restricted to previously described DLBCL driver genes (38,40), listed in
628 **Supplementary Table 2.** Maftools (v2.12.0) was used to compare alterations between groups,
629 where additional filtering was performed to filter to genes altered in at least 10% of samples of the
630 smaller group (93).
631
632 **Mutational pathway analysis**
633 Genes in the BCR-dependent NFKB pathway (44,45) and cell cycle pathway-related genes (45)
634 were curated from previously published studies. The proportion of patients with an alteration in at
635 least one gene in the pathway was calculated and compared across clusters. Alterations for a given
636 gene were filtered to reflect their putative role as an oncogene or as a tumor suppressor gene.
637
638 **CIBERSORTx**
639 Immune cell deconvolution was performed using CIBERSORTx using the LM22 signature
640 matrix(47,94). The software was run on bulk-mode and absolute mode. For the input mixture file,
641 RNA-seq counts were first batch corrected using ComBat-Seq followed by quantification to
642 transcripts per million (TPM) (95).
643
644 Cell types were condensed as such:

645 **T.cells** = "T cells CD8" + "T cells follicular helper ($T_{fh}$)" + "T cells regulatory (Tregs)" + "T cells
646 CD4 naïve" + "T cells CD4 memory resting" + "T cells CD4 memory activated"+ "T cells gamma
647 delta"
648 **NK.cells** = "NK cells activated" + "NK cells resting"
649 **Memory.CD4.T.cells** = "T cells CD4 memory resting" + "T cells CD4 memory activated"
650 **Conv.CD4.T.cells** = "Memory.CD4.T.cells" + "T cells CD4 naïve" + "T cells follicular helper"
651 **CD4.T.cells** = "Memory.CD4.T.cells" + "T cells CD4 naïve" + "T cells follicular helper" + "T
652 cells regulatory ($T_{regs}$)"
653 **Dendritic.cells** = "Dendritic cells activated" + "Dendritic cells resting"
654 **B.cells** = "B cells naïve" + "B cells memory" + "Plasma cells"
655 **Macrophages** = "Macrophages M0" + "Macrophages M1" + "Macrophages M2"
656
657 EcoTyper (https://github.com/digitalcytometry/ecotype) was used to recover previously defined
658 Lymphoma Ecotypes; input data were quantified as TPM (96).
659
660 **Gene set compilation**
661 Gene sets were manually curated following an extensive literature search and focused on genes
662 related to 1) immune cell infiltration and activation, 2) cell-of-origin and 3) key transcription
663 factors related to cell-of-origin. Gene sets were excluded if they had fewer than 3 or more than 200
664 genes. Genes included in each gene set are listed in **Supplementary Table 1**.
665
666 ***Immune-related gene sets***: Twelve immune-related gene sets were included, known to be
667 associated with immune activity in other cancer types. Gene sets were related to activation state of

668 T cells (t.cell.activation (11), t.cell.exhaustion (11), IFNγ_ayers (8)), non-cellular mediators of
669 immune responses (ifn1_rooney (11), cytolytic.score (23)), and presence of immune cell subsets
670 (tfh_charoentong (22), th1_charoentong (22), th2_charoentong (22), treg_rooney (11),
671 cd8t_charoentong (22), macrophage_rooney (11), dc_xcell_total (24)). In general, immune-related
672 gene sets had less than 15% overlap based on pairwise comparisons.
673
674 ***Cell of origin gene sets*:** A total of four COO gene sets - 2 ABC DLBCL (ABCDLBC-1,
675 ABCDLBCL-2) specific gene sets and 2 GCB DLBCL specific gene sets (GCBDLBCL-1,
676 GCBDLBCL-2) - were included. Gene sets are derived from the seminal gene expression classifier
677 (25), found in SignatureDB (SigDB)(46). (https://lymphochip.nih.gov/signaturedb/index.html).
678
679 ***Transcription factor gene sets***: Three transcription factor related gene sets – related to IRF4
680 (IRF4Up-7 and IRF4Dn-1) and BCL6 (BCL6Dn-1) targets – were included from SigDB (46).
681
682 **Immune signature clustering model**
683 Gene set variation analysis (GSVA) using the 19 curated gene sets was performed on bulk
684 transcriptomes from 2 genomic datasets (NCI, n = 481; UCMC, n = 96) (18,20). The resulting
685 GSVA scores were resolved using principal component analysis (PCA). Unsupervised k-means
686 clustering was utilized to assign samples into unique clusters, where k = 4 clusters was optimally
687 selected using an elbow plot. Subsequent analyses using the third independent BCC dataset as well
688 as the 3-dataset combination were performed in the same structured steps, where equivalent
689 clustering was observed.
690

691 **Generation of MYCUp4 expression groups**

692 GSVA scores for the MYCUp-4 gene set (from SigDB (46)) were generated for all DLBCLs in
693 UCMC, NCI, and BCC datasets. DLBCLs were then split into ABC and GCB groups based on
694 their immune-related cluster membership, and a 25-75 percentile split within each COO group was
695 used to assign DLBCLs to "MYC-High" and "MYC-Low" groups. All other DLBCLs were
696 assigned to the "MYC-Int" group.

697

698 **Multispectral immunofluorescence**

699 Multi-spectral immunofluorescence (mIF) microscopy was performed on 65 DLBCLs (UCMC)
700 for which paired RNA-seq and GSVA data were available. mIF analysis was performed after
701 staining with fluorescence-labeled antibodies against a T cell panel and myeloid cell panel *(see*
702 *antibodies for mIF section*). Each slide was scanned using the Vectra Polaris (Akoya Biosciences)
703 imaging platform and the Phenochart software (PerkinElmer). Through Phenochart, at least 5
704 representative regions of interest per tissue section were acquired as multispectral images at 40x
705 magnification. Watershed segmentation was used to identify nuclei using DAPI staining and cell
706 borders of individual cells in each ROI. The supervised machine-learning algorithm in the inForm
707 software (v. 2.3) was used to classify each cell into specific phenotypes.

708 1. Slides were divided by panel and by specific features determined during the initial
709 watershed segmentation, including cell border detection, average cell size,
710 autofluorescence, and DAPI strength.
711 2. Samples were divided into 4 separate groups for each panel. 2 ROIs were chosen per
712 sample to train the machine-learning algorithm in inForm to identify the following
713 phenotypes with the associated markers:

714 1. **T cells** : $CD8^+$ T cell, $CD4^+$ T cell, $PAX5^+$ DLBCL cell

715 2. **Myeloid cells** : $CD68^+$ Macrophage, $CD11c^+$ dendritic cell

716 3. Once the initial training groups were processed, all ROIs in each group of samples were

717 classified using the matching training cohort.

718 4. Results of per-slide frequencies of each phenotype were tabulated in R using exported

719 values from inForm using the `phenoptr` package and the representative mIF images were

720 also exported through inForm. Given heterogeneity of tumor and microenvironment

721 composition in each ROI, comparisons were made between total number of each TME cell

722 population/phenotype normalized against the number of DLBCL cells present across all

723 ROIs per slide.

724

725 **Antibodies for mIF**

726

| | | | | | | |
|---|---|---|---|---|---|---|
| PAX5 | nucleus | 620 | BioCare Medical,CM 207 | BC/24, mouse mAb | AR9 | 1:50 in Da Vinci Green |
| CD68 | membrane+cytoplasmic | 570 | BioCare Medical, CM033A | KP1, mouse mAb | AR9 | 1:50 in Da Vinci Green |
| CD11c | membrane | 540 | BioCare Medical, ACI3122A | 5D11, mouse mAB | AR9 | 1:100 in Renoir Red |

727

728

| | | | | | | |
|---|---|---|---|---|---|---|
| CD4 | membrane | 520 | BioCare Medical, ACI3148A | 4B12, mouse mAb | AR9 | 1:50 in Van Gogh Yellow |
| PAX5 | nucleus | 620 | BioCare Medical,CM 207 | BC/24, mouse mAb | AR9 | 1:50 in Da Vinci Green |

| | | | | | | |
|---|---|---|---|---|---|---|
| CD8 | membrane | 690 | R&D, NBP232836B | C8/144B, mouse mAb | AR9 | 1:50 |

729

730 ***In vitro* IFNγ stimulation of splenocytes**

731 Spleens from *CD19*$^{Cre/wt}$ and *CD19*$^{Cre/wt}$ ; *Socs1*$^{fl/fl}$ mice were obtained from Ari Melnick (Weill
732 Cornell Medicine). Spleens were passed through a 70 µm cell strainer (Corning, 352350) and
733 ground using the plunger of a syringe with 10 mL of PBS to yield single cell suspensions.
734 Splenocytes were then washed twice in 10mL of PBS, followed by lysis of red blood cells in a
735 hypotonic solution and three washes in 10 mL of PBS. 5 x $10^5$ splenocytes from single cell
736 suspensions were incubated with increasing concentrations of recombinant mouse IFNγ (0, 0.1, 1,
737 10, 100 ng/mL) for 48 hours (Peprotech, 315-05). Cells were then harvested and incubated with a
738 panel of antibodies containing anti-mouse CD19 (Biolegend,115504), anti-mouse CD3d
739 (Biolegend, 100244), anti-mouse H-2 (Biolegend, 125506), anti-mouse I-A/I-E (Biolegend,
740 107619), and anti-mouse PD-L1 (Biolegend, 124311). Splenocytes were analyzed by flow
741 cytometry for expression of H-2, I-A/I-E, and PD-L1 on $CD19^+$ and $CD3^+$ cell populations. Mean
742 fluorescence intensity (MFI) fold change for H-2, H-2, I-A/I-E, and PD-L1 was computed by
743 comparing treatment with IFNγ compared to media-only control. Data shown are the average of at
744 least 3 independent biological replicates. Statistical testing was conducted using a 2-way ANOVA
745 with Bonferroni correction for multiple comparisons.

746

747 **Statistical methods**

748 All statistical analyses were performed in R (v4.2.1). Statistical significance for categorical
749 variables was assessed with a Fisher's exact test for two-group comparisons; a multi-way Fisher's
750 exact test followed by post-hoc individual pairwise testing was used for comparisons of three or

more groups. Statistical significance of continuous variables was performed with a Mann-Whitney U test for two-group comparisons and a Kruskal-Wallis test followed by a post-hoc Dunn's test for comparisons across three or more groups. Survival analysis was performed using the survival package (v3.4.0), and the log-rank test was used to determine significance. A p value threshold of 0.05 was used to assess univariate statistical significance. Adjustment for multiple hypothesis testing was performed using the Benjamini-Hochberg method unless indicated otherwise.

## References


1. Neelapu SS, Locke FL, Bartlett NL, Lekakis LJ, Miklos DB, Jacobson CA, et al. Axicabtagene Ciloleucel CAR T-Cell Therapy in Refractory Large B-Cell Lymphoma. N Engl J Med. 2017;377:2531–44.

2. Locke FL, Miklos DB, Jacobson CA, Perales M-A, Kersten M-J, Oluwole OO, et al. Axicabtagene Ciloleucel as Second-Line Therapy for Large B-Cell Lymphoma. N Engl J Med. Massachusetts Medical Society; 2022;386:640–54.

3. Schuster SJ, Bishop MR, Tam CS, Waller EK, Borchmann P, McGuirk JP, et al. Tisagenlecleucel in Adult Relapsed or Refractory Diffuse Large B-Cell Lymphoma. https://doi.org/101056/NEJMoa1804980. Massachusetts Medical Society; 2018;380:45–56.

4. Abramson JS, Palomba ML, Gordon LI, Lunning MA, Wang M, Arnason J, et al. Lisocabtagene maraleucel for patients with relapsed or refractory large B-cell lymphomas (TRANSCEND NHL 001): a multicentre seamless design study. The Lancet. Elsevier; 2020;396:839–52.

5. Budde LE, Assouline S, Sehn LH, Schuster SJ, Yoon S-S, Yoon DH, et al. Single-Agent Mosunetuzumab Shows Durable Complete Responses in Patients With Relapsed or Refractory B-Cell Lymphomas: Phase I Dose-Escalation Study. J Clin Oncol. Wolters Kluwer; 2022;40:481–91.

779 6. Dickinson MJ, Carlo-Stella C, Morschhauser F, Bachy E, Corradini P, Iacoboni G, et al.
780 Glofitamab for Relapsed or Refractory Diffuse Large B-Cell Lymphoma. N Engl J Med.
781 Massachusetts Medical Society; 2022;387:2220–31.

782 7. Thieblemont C, Phillips T, Ghesquieres H, Cheah CY, Clausen MR, Cunningham D, et al.
783 Epcoritamab, a Novel, Subcutaneous CD3xCD20 Bispecific T-Cell–Engaging Antibody, in
784 Relapsed or Refractory Large B-Cell Lymphoma: Dose Expansion in a Phase I/II Trial. J
785 Clin Oncol. Wolters Kluwer; 2023;41:2238–47.

786 8. Ayers M, Lunceford J, Nebozhyn M, Murphy E, Loboda A, Kaufman DR, et al. IFN-γ-
787 related mRNA profile predicts clinical response to PD-1 blockade. J Clin Invest. American
788 Society for Clinical Investigation; 2017;127:2930–40.

789 9. Ott PA, Bang Y-J, Piha-Paul SA, Razak ARA, Bennouna J, Soria J-C, et al. T-Cell–Inflamed
790 Gene-Expression Profile, Programmed Death Ligand 1 Expression, and Tumor Mutational
791 Burden Predict Efficacy in Patients Treated With Pembrolizumab Across 20 Cancers:
792 KEYNOTE-028. J Clin Oncol. Wolters Kluwer; 2019;37:318–27.

793 10. Thorsson V, Gibbs DL, Brown SD, Wolf D, Bortone DS, Ou Yang T-H, et al. The Immune
794 Landscape of Cancer. Immunity. 2018;48:812-830.e14.

795 11. Rooney MS, Shukla SA, Wu CJ, Getz G, Hacohen N. Molecular and Genetic Properties of
796 Tumors Associated with Local Immune Cytolytic Activity. 2015; Available from:
797 http://dx.doi.org/10.1016/j.cell.2014.12.033

798 12. Monti S, Savage KJ, Kutok JL, Feuerhake F, Kurtin P, Mihm M, et al. Molecular profiling of
799 diffuse large B-cell lymphoma identifies robust subtypes including one characterized by
800 host inflammatory response. Blood. 2005;105:1851–61.

801 13. Alizadeh AA, Eisen MB, Davis RE, Ma C, Lossos IS, Rosenwald A, et al. Distinct types of
802 diffuse large B-cell lymphoma identified by gene expression profiling. Nature.
803 2000;403:503–11.

804 14. Lenz G, Wright G, Dave SS, Xiao W, Powell J, Zhao H, et al. Stromal gene signatures in
805 large-B-cell lymphomas. N Engl J Med. 2008;359:2313–23.

806 15. Kotlov N, Bagaev A, Revuelta MV, Phillip JM, Cacciapuoti MT, Antysheva Z, et al. Clinical
807 and Biological Subtypes of B-cell Lymphoma Revealed by Microenvironmental Signatures.
808 Cancer Discov. 2021;11:1468–89.

809 16. Ansell SM. Checkpoint Blockade in Lymphoma. J Clin Oncol [Internet]. American Society
810 of Clinical Oncology; 2021 [cited 2023 Feb 23]; Available from:
811 https://ascopubs.org/doi/pdf/10.1200/JCO.20.01522?role=tab

812 17. Kline J, Godfrey J, Ansell SM. The immune landscape and response to immune checkpoint
813 blockade therapy in lymphoma. Blood. 2020;135:523–33.

814 18. Wright GW, Huang DW, Phelan JD, Coulibaly ZA, Roulland S, Young RM, et al. A
815 Probabilistic Classification Tool for Genetic Subtypes of Diffuse Large B Cell Lymphoma
816 with Therapeutic Implications. Cancer Cell. Cell Press; 2020;37:551-568.e14.

817 19. Schmitz R, Wright GW, Huang DW, Johnson CA, Phelan JD, Wang JQ, et al. Genetics and
818 Pathogenesis of Diffuse Large B-Cell Lymphoma. N Engl J Med. Massachusetts Medical
819 Society; 2018;378:1396–407.

820 20. Godfrey J, Tumuluru S, Bao R, Leukam M, Venkataraman G, Phillip J, et al. PD-L1 gene
821 alterations identify a subset of diffuse large B-cell lymphoma harboring a T-cell–inflamed
822 phenotype. Blood. American Society of Hematology; 2019;133:2279–90.

823 21. Hänzelmann S, Castelo R, Guinney J. GSVA: gene set variation analysis for microarray and
824 RNA-Seq data. BMC Bioinformatics. 2013;14:7.

825 22. Charoentong P, Finotello F, Angelova M, Mayer C, Efremova M, Rieder D, et al. Pan-cancer
826 Immunogenomic Analyses Reveal Genotype-Immunophenotype Relationships and
827 Predictors of Response to Checkpoint Blockade. Cell Rep. 2017;18:248–62.

828 23. Dufva O, Pölönen P, Brück O, Keränen MAI, Klievink J, Mehtonen J, et al. Immunogenomic
829 Landscape of Hematological Malignancies. Cancer Cell. 2020;38:380-399.e13.

830 24. Aran D, Hu Z, Butte AJ. xCell: Digitally portraying the tissue cellular heterogeneity
831 landscape. Genome Biol. 2017;18.

832 25. Wright G, Tan B, Rosenwald A, Hurt EH, Wiestner A, Staudt LM. A gene expression-based
833 method to diagnose clinically distinct subgroups of diffuse large B cell lymphoma. Proc
834 Natl Acad Sci U S A. 2003;100:9991–6.

835 26. Yang Y, Shaffer AL, Emre NCT, Ceribelli M, Zhang M, Wright G, et al. Exploiting
836 Synthetic Lethality for the Therapy of ABC Diffuse Large B Cell Lymphoma. Cancer Cell.
837 2012;21:723–37.

838 27. Duns G, Viganò E, Ennishi D, Sarkozy C, Hung SS, Chavez E, et al. Characterization of
839 DLBCL with a PMBL gene expression signature. Blood. American Society of Hematology;
840 2021;138:136–48.

841 28. Ennishi D, Jiang A, Boyle M, Collinge B, Grande BM, Ben-Neriah S, et al. Double-Hit Gene
842 Expression Signature Defines a Distinct Subgroup of Germinal Center B-Cell-Like Diffuse
843 Large B-Cell Lymphoma. J Clin Oncol. 2019;37:190–201.

844 29. Spranger S, Bao R, Gajewski TF. Melanoma-intrinsic β-catenin signalling prevents anti-
845 tumour immunity. Nature. Nature Publishing Group; 2015;523:231–5.

846 30. Ennishi D, Takata K, Béguelin W, Duns G, Mottok A, Farinha P, et al. Molecular and
847 genetic characterization of MHC deficiency identifies ezh2 as therapeutic target for
848 enhancing immune recognition. Cancer Discov. American Association for Cancer Research
849 Inc.; 2019;9:546–63.

850 31. Shouval R, Alarcon Tomas A, Fein JA, Flynn JR, Markovits E, Mayer S, et al. Impact of
851 TP53 Genomic Alterations in Large B-Cell Lymphoma Treated With CD19-Chimeric
852 Antigen Receptor T-Cell Therapy. J Clin Oncol. Wolters Kluwer; 2022;40:369–81.

853 32. Peng W, Chen JQ, Liu C, Malu S, Creasy C, Tetzlaff MT, et al. Loss of PTEN Promotes
854 Resistance to T Cell-Mediated Immunotherapy. Cancer Discov. 2016;6:202–16.

855 33. Peng D, Kryczek I, Nagarsheth N, Zhao L, Wei S, Wang W, et al. Epigenetic silencing of
856 TH1-type chemokines shapes tumour immunity and immunotherapy. Nature. Nature
857 Publishing Group; 2015;527:249–53.

858 34. Manguso RT, Pope HW, Zimmer MD, Brown FD, Yates KB, Miller BC, et al. In vivo
859 CRISPR screening identifies Ptpn2 as a cancer immunotherapy target. Nature. Nature
860 Publishing Group; 2017;547:413–8.

861 35. Pan D, Kobayashi A, Jiang P, Ferrari de Andrade L, Tay RE, Luoma AM, et al. A major
862 chromatin regulator determines resistance of tumor cells to T cell–mediated killing.
863 Science. 2018;359:770–5.

864 36. Wellenstein MD, de Visser KE. Cancer-Cell-Intrinsic Mechanisms Shaping the Tumor
865 Immune Landscape. Immunity. 2018;48:399–416.

866 37. Spranger S, Gajewski TF. Mechanisms of Tumor Cell–Intrinsic Immune Evasion. Annu Rev
867 Cancer Biol. 2018;2:213–28.

868 38. Chapuy B, Stewart C, Dunford AJ, Kim J, Kamburov A, Redd RA, et al. Molecular subtypes
869 of diffuse large B cell lymphoma are associated with distinct pathogenic mechanisms and
870 outcomes. Nat Med. Nature Publishing Group; 2018;24:679–90.

871 39. Lacy SE, Barrans SL, Beer PA, Painter D, Smith AG, Roman E, et al. Targeted sequencing
872 in DLBCL, molecular subtypes, and outcomes: a Haematological Malignancy Research
873 Network report. Blood. 2020;135:1759–71.

874 40. Reddy A, Zhang J, Davis NS, Moffitt AB, Love CL, Waldrop A, et al. Genetic and
875 Functional Drivers of Diffuse Large B Cell Lymphoma. Cell. Cell Press; 2017;171:481-
876 494.e15.

877 41. Ennishi D, Healy S, Bashashati A, Saberi S, Hother C, Mottok A, et al. TMEM30A loss-of-
878 function mutations drive lymphomagenesis and confer therapeutically exploitable
879 vulnerability in B-cell lymphoma. Nat Med. Nature Research; 2020;26:577–88.

880 42. Venturutti L, Teater M, Zhai A, Chadburn A, Babiker L, Kim D, et al. TBL1XR1 Mutations
881 Drive Extranodal Lymphoma by Inducing a Pro-tumorigenic Memory Fate. Cell.
882 2020;182:297-316.e27.

883 43. Young RM, Shaffer AL, Phelan JD, Staudt LM. B cell Receptor Signaling in Diffuse Large
884 B cell Lymphoma. Semin Hematol. 2015;52:77–85.

885 44. Phelan JD, Young RM, Webster DE, Roulland S, Wright GW, Kasbekar M, et al. A
886 multiprotein supercomplex controlling oncogenic signalling in lymphoma. Nature. Nature
887 Publishing Group; 2018;560:387–91.

888 45. Miao Y, Medeiros LJ, Li Y, Li J, Young KH. Genetic alterations and their clinical
889 implications in DLBCL. Nat Rev Clin Oncol. Nature Publishing Group; 2019;16:634–52.

890 46. Shaffer AL, Wright G, Yang L, Powell J, Ngo V, Lamy L, et al. A library of gene expression
891 signatures to illuminate normal and pathological lymphoid biology. Immunol Rev.
892 2006;210:67–85.

893 47. Newman AM, Steen CB, Liu CL, Gentles AJ, Chaudhuri AA, Scherer F, et al. Determining
894 cell type abundance and expression from bulk tissues with digital cytometry. Nat
895 Biotechnol. Nature Publishing Group; 2019;37:773–82.

896 48. Green MR, Monti S, Rodig SJ, Juszczynski P, Currie T, O'Donnell E, et al. Integrative
897 analysis reveals selective 9p24.1 amplification, increased PD-1 ligand expression, and
898 further induction via JAK2 in nodular sclerosing Hodgkin lymphoma and primary
899 mediastinal large B-cell lymphoma. Blood. 2010;116:3268–77.

900 49. Wienand K, Chapuy B, Stewart C, Dunford AJ, Wu D, Kim J, et al. Genomic analyses of
901 flow-sorted Hodgkin Reed-Sternberg cells reveal complementary mechanisms of immune
902 evasion. Blood Adv. American Society of Hematology; 2019;3:4065–80.

903 50. Reichel J, Chadburn A, Rubinstein PG, Giulino-Roth L, Tam W, Liu Y, et al. Flow sorting
904 and exome sequencing reveal the oncogenome of primary Hodgkin and Reed-Sternberg
905 cells. Blood. American Society of Hematology; 2015;125:1061–72.

906 51. Chapuy B, Stewart C, Dunford AJ, Kim J, Wienand K, Kamburov A, et al. Genomic
907 analyses of PMBL reveal new drivers and mechanisms of sensitivity to PD-1 blockade.
908 Blood. American Society of Hematology; 2019;134:2369–82.

909 52. Mottok A, Hung SS, Chavez EA, Woolcock B, Telenius A, Chong LC, et al. Integrative
910 genomic analysis identifies key pathogenic mechanisms in primary mediastinal large B-cell
911 lymphoma. Blood. American Society of Hematology; 2019;134:802–13.

912 53. Noerenberg D, Briest F, Hennch C, Yoshida K, Hablesreiter R, Takeuchi Y, et al. Genetic
913 Characterization of Primary Mediastinal B-Cell Lymphoma: Pathogenesis and Patient
914 Outcomes. J Clin Oncol. Wolters Kluwer; 2023;JCO.23.01053.

915 54. Ansell SM, Lesokhin AM, Borrello I, Halwani A, Scott EC, Gutierrez M, et al. PD-1
916 Blockade with Nivolumab in Relapsed or Refractory Hodgkin's Lymphoma. N Engl J Med.
917 2015;372:311–9.

918 55. Armand P, Rodig S, Melnichenko V, Thieblemont C, Bouabdallah K, Tumyan G, et al.
919 Pembrolizumab in Relapsed or Refractory Primary Mediastinal Large B-Cell Lymphoma.
920 https://doi.org/101200/JCO1901389. American Society of Clinical Oncology;
921 2019;37:3291–9.

922 56. Armand P, Engert A, Younes A, Fanale M, Santoro A, Zinzani PL, et al. Nivolumab for
923 Relapsed/Refractory Classic Hodgkin Lymphoma After Failure of Autologous
924 Hematopoietic Cell Transplantation: Extended Follow-Up of the Multicohort Single-Arm
925 Phase II CheckMate 205 Trial. J Clin Oncol. 2018;36:1428–39.

926 57. Aoki T, Chong LC, Takata K, Milne K, Hav M, Colombo A, et al. Single-cell transcriptome
927 analysis reveals disease-defining t-cell subsets in the tumor microenvironment of classic
928 hodgkin lymphoma. Cancer Discov. American Association for Cancer Research Inc.;
929 2020;10:406–21.

930 58. Melzner I, Bucur AJ, Brüderlein S, Dorsch K, Hasel C, Barth TFE, et al. Biallelic mutation
931 of SOCS-1 impairs JAK2 degradation and sustains phospho-JAK2 action in the MedB-1
932 mediastinal lymphoma line. Blood. 2005;105:2535–42.

933 59. Savage KJ, Monti S, Kutok JL, Cattoretti G, Neuberg D, De Leval L, et al. The molecular
934 signature of mediastinal large B-cell lymphoma differs from that of other diffuse large B-
935 cell lymphomas and shares features with classical Hodgkin lymphoma. Blood.
936 2003;102:3871–9.

937 60. Viganò E, Gunawardana J, Mottok A, Van Tol T, Mak K, Chan FC, et al. Somatic IL4R
938 mutations in primary mediastinal large B-cell lymphoma lead to constitutive JAK-STAT
939 signaling activation. Blood. 2018;131:2036–46.

940 61. Alexander WS, Starr R, Fenner JE, Scott CL, Handman E, Sprigg NS, et al. SOCS1 is a
941 critical inhibitor of interferon γ signaling and prevents the potentially fatal neonatal actions
942 of this cytokine. Cell. Elsevier B.V.; 1999;98:597–608.

943 62. Liau NPD, Laktyushin A, Lucet IS, Murphy JM, Yao S, Whitlock E, et al. The molecular
944 basis of JAK/STAT inhibition by SOCS1. Nat Commun 2018 91. Nature Publishing Group;
945 2018;9:1–14.

946 63. Horvath CM. The Jak-STAT Pathway Stimulated by Interferon γ. Sci STKE. American
947 Association for the Advancement of Science; 2004;2004:tr8–tr8.

948 64. Villarino AV, Kanno Y, O'Shea JJ. Mechanisms and consequences of Jak–STAT signaling
949 in the immune system. Nat Immunol. Nature Publishing Group; 2017;18:374–84.

950 65. Ivashkiv LB. IFNγ: signalling, epigenetics and roles in immunity, metabolism, disease and
951 cancer immunotherapy. Nat Rev Immunol. 2018;18:545–58.

952 66. Hugo W, Zaretsky JM, Sun L, Song C, Moreno BH, Hu-Lieskovan S, et al. Genomic and
953 Transcriptomic Features of Response to Anti-PD-1 Therapy in Metastatic Melanoma. Cell.
954 2016;165:35–44.

955 67. Kalbasi A, Ribas A. Tumour-intrinsic resistance to immune checkpoint blockade. Nat Rev
956 Immunol. 2020;20:25–39.

957 68. Sworder BJ, Kurtz DM, Alig SK, Frank MJ, Shukla N, Garofalo A, et al. Determinants of
958 resistance to engineered T cell therapies targeting CD19 in large B cell lymphomas. Cancer
959 Cell. Elsevier; 2023;41:210-225.e5.

960 69. Locke FL, Filosto S, Chou J, Vardhanabhuti S, Perbost R, Dreger P, et al. Impact of tumor
961 microenvironment on efficacy of anti-CD19 CAR T cell therapy or chemotherapy and
962 transplant in large B cell lymphoma. Nat Med. Nature Publishing Group; 2024;1–12.

963 70. Yoshimura A, Naka T, Kubo M. SOCS proteins, cytokine signalling and immune regulation.
964 Nat Rev Immunol 2007 76. Nature Publishing Group; 2007;7:454–65.

965 71. Patel SJ, Sanjana NE, Kishton RJ, Eidizadeh A, Vodnala SK, Cam M, et al. Identification of
966 essential genes for cancer immunotherapy. Nature. Nature Publishing Group;
967 2017;548:537–42.

968 72. Wee ZN, Li Z, Lee PL, Lee ST, Lim YP, Yu Q. EZH2-Mediated Inactivation of IFN-γ-JAK-
969 STAT1 Signaling Is an Effective Therapeutic Target in MYC-Driven Prostate Cancer. Cell
970 Rep. Elsevier; 2014;8:204–16.

971 73. Zaretsky JM, Garcia-Diaz A, Shin DS, Escuin-Ordinas H, Hugo W, Hu-Lieskovan S, et al.
972 Mutations Associated with Acquired Resistance to PD-1 Blockade in Melanoma.
973 https://doi.org/101056/NEJMoa1604958. Massachusetts Medical Society; 2016;375:819–
974 29.

975 74. Gao J, Shi LZ, Zhao H, Chen J, Xiong L, He Q, et al. Loss of IFN-γ Pathway Genes in
976 Tumor Cells as a Mechanism of Resistance to Anti-CTLA-4 Therapy. Cell. 2016;167:397-
977 404.e9.

978 75. Baumgartner CK, Ebrahimi-Nik H, Iracheta-Vellve A, Hamel KM, Olander KE, Davis TGR,
979 et al. The PTPN2/PTPN1 inhibitor ABBV-CLS-484 unleashes potent anti-tumour
980 immunity. Nature. Nature Publishing Group; 2023;622:850–62.

981 76. Miao D, Margolis CA, Gao W, Voss MH, Li W, Martini DJ, et al. Genomic correlates of
982 response to immune checkpoint therapies in clear cell renal cell carcinoma. Science.
983 2018;806:801–6.

984 77. Choi J, Phelan JD, Wright GW, Häupl B, Huang DW, Shaffer AL, et al. Regulation of B cell
985 receptor-dependent NF-κB signaling by the tumor suppressor KLHL14. Proc Natl Acad
986 Sci. Proceedings of the National Academy of Sciences; 2020;117:6092–102.

987 78. Staudt LM. Oncogenic Activation of NF-κB. Cold Spring Harb Perspect Biol.
988 2010;2:a000109.

989 79. Ott G, Rosenwald A, Campo E. Understanding MYC-driven aggressive B-cell lymphomas:
990 pathogenesis and classification. Blood. 2013;122:3884–91.

991 80. Copie-Bergman C, Cuillière-Dartigues P, Baia M, Briere J, Delarue R, Canioni D, et al.
992 MYC-IG rearrangements are negative predictors of survival in DLBCL patients treated
993 with immunochemotherapy: a GELA/LYSA study. Blood. 2015;126:2466–74.

994 81. Friedberg JW. Double-Hit Diffuse Large B-Cell Lymphoma. J Clin Oncol. Wolters Kluwer;
995 2012;30:3439–43.

996 82. Shen R, Seshan VE. FACETS: allele-specific copy number and clonal heterogeneity analysis
997 tool for high-throughput DNA sequencing. Nucleic Acids Res. 2016;44:e131.

998 83. Chen S, Zhou Y, Chen Y, Gu J. fastp: an ultra-fast all-in-one FASTQ preprocessor.
999 Bioinformatics. 2018;34:i884–90.

1000 84. Li H, Durbin R. Fast and accurate short read alignment with Burrows-Wheeler transform.
1001 Bioinformatics. 2009;25:1754–60.

1002 85. Van der Auwera GA, Carneiro MO, Hartl C, Poplin R, del Angel G, Levy-Moonshine A, et
1003 al. From FastQ data to high confidence variant calls: the Genome Analysis Toolkit best
1004 practices pipeline. Curr Protoc Bioinforma Ed Board Andreas Baxevanis Al.
1005 2013;11:11.10.1-11.10.33.

1006 86. Saunders CT, Wong WSW, Swamy S, Becq J, Murray LJ, Cheetham RK. Strelka: accurate
1007 somatic small-variant calling from sequenced tumor–normal sample pairs. Bioinformatics.
1008 2012;28:1811–7.

1009 87. Dunn T, Berry G, Emig-Agius D, Jiang Y, Lei S, Iyer A, et al. Pisces: an accurate and
1010 versatile variant caller for somatic and germline next-generation sequencing data.
1011 Bioinformatics. 2019;35:1579–81.

1012 88. McLaren W, Gil L, Hunt SE, Riat HS, Ritchie GRS, Thormann A, et al. The Ensembl
1013 Variant Effect Predictor. Genome Biol. 2016;17:122.

1014 89. Favero F, Joshi T, Marquard AM, Birkbak NJ, Krzystanek M, Li Q, et al. Sequenza: allele-
1015 specific copy number and mutation profiles from tumor sequencing data. Ann Oncol.
1016 Elsevier; 2015;26:64–70.

1017 90. Bray NL, Pimentel H, Melsted P, Pachter L. Near-optimal probabilistic RNA-seq
1018 quantification. Nat Biotechnol. Nature Publishing Group; 2016;34:525–7.

1019 91. Law CW, Chen Y, Shi W, Smyth GK. voom: precision weights unlock linear model analysis
1020 tools for RNA-seq read counts. Genome Biol. 2014;15:R29.

1021 92. Subramanian A, Tamayo P, Mootha VK, Mukherjee S, Ebert BL, Gillette MA, et al. Gene
1022 set enrichment analysis: a knowledge-based approach for interpreting genome-wide
1023 expression profiles. Proc Natl Acad Sci U S A. National Academy of Sciences;
1024 2005;102:15545–50.

1025 93. Mayakonda A, Lin D-C, Assenov Y, Plass C, Koeffler HP. Maftools: efficient and
1026 comprehensive analysis of somatic variants in cancer. Genome Res. 2018;28:1747–56.

1027 94. Newman AM, Liu CL, Green MR, Gentles AJ, Feng W, Xu Y, et al. Robust enumeration of
1028 cell subsets from tissue expression profiles. Nat Methods. Nature Publishing Group;
1029 2015;12:453–7.

1030 95. Zhang Y, Parmigiani G, Johnson WE. ComBat-seq: batch effect adjustment for RNA-seq
1031 count data. NAR Genomics Bioinforma. 2020;2:lqaa078.

1032 96. Steen CB, Luca BA, Esfahani MS, Azizi A, Sworder BJ, Nabet BY, et al. The landscape of
1033 tumor cell states and ecosystems in diffuse large B cell lymphoma. Cancer Cell [Internet].
1034 2021; Available from: https://linkinghub.elsevier.com/retrieve/pii/S1535610821004517